ORIGINAL CONTRIBUTION

Cation release from different carboxymethyl cellulose hydrogels

Yi Qu[1,2] · René Haverkamp[1] · Désirée Jakobs-Schönwandt[2] · Jorge Miguel Esteban Vazquez[1] · Thomas Hellweg[1] · Anant V. Patel[2]

Abstract

Biodegradable hydrogels have great potential in agriculture. In this study, hydrogel prototypes of biodegradable slow-release fertilizers were formulated by a Schiff base reaction between dialdehyde carboxymethyl cellulose and gelatin. The release behavior of iron cations from these carboxymethyl cellulose-based hydrogels with different degrees of substitution was studied. The analyses of the relation between correlation length of the cross-linked hydrogels and the degree of substitution, i.e., the amount of negatively charged positions in the hydrogels, allowed to determine the influence of structure and electrostatic interaction on cation release kinetics, which was successfully described by Peleg's Model. The hydrogel with the lowest degree of substitution reveals the slowest release of cations due to the smallest correlation length. These results demonstrate that the correlation length is dominant for the release of divalent cations. Moreover, this also shows the potential of the DACMC-Gelatin hydrogels as matrix for slow-release fertilizers.

Keywords Slow-release fertilizer · Schiff base reaction · Hydrogel · Release kinetics · Correlation length · SAXS

Introduction

The world population is expected to reach 8.1 billion in 2025 and 9.6 billion in 2050 [1, 2]. Meanwhile, the recent "Global Report on Food Crises 2022" warned that about 193 million people in 53 countries are severely food insecure [3]. Fertilizer use is increasing by 2.5 million tons per year to improve food production and close the supply gap [4–6]. However, unformulated fertilizers release nutrients rapidly, resulting in severe environmental pollution, such as eutrophication of water bodies, groundwater pollution, or emission of greenhouse gasses [5, 7, 8]. Meanwhile, the use of macronutrient fertilizers has led to the deficiency of secondary and micronutrients such as zinc (Zn), iron (Fe), and manganese

(Mn) in the soil, which has been already observed in some intensively planted areas [9–11]. Attempts to formulate fertilizers often make use of non-degradable materials such as polyolefins, resins, or polyurethanes, which may lead to the accumulation of toxic substances in soil [12, 13].

Therefore, research on slow release fertilizers (SRF) with biodegradable biobased materials, such as alginate, chitosan, gelatin, cellulose, starch, and soy proteins, has been considered for decades [14–16]. These fertilizers slowly release the nutrients and thus reduce wash-out in comparison to non-formulated fertilizers, while formulation materials can be slowly decomposed by microbial decomposition, photolysis, or hydrolysis in the soil [13, 17–19].

Among these degradable materials, gelatin and cellulose are the two candidates with the greatest potential because they are environmentally friendly, abundant, and renewable [16]. Gelatin is a derivate of collagen, but it has better water solubility and amphoteric behavior due to the coexisting alkaline amino groups ($-NH_2$) and acidic carboxyl groups ($-COOH$) in the linear structure. The safety and biodegradability of gelatin have been confirmed by the Food and Drug Administration (FDA) [20]. Two types of gelatins are produced by different processes. Type A gelatin is produced by acidic preconditions and has an isoelectric point (IEP) around 9.00, while type B gelatin is obtained under alkaline conditions and has

✉ Thomas Hellweg
  thomas.hellweg@uni-bielefeld.de

✉ Anant V. Patel
  anant.patel@fh-bielefeld.de

1   Department of Chemistry, Physical and Biophysical Chemistry, Bielefeld University, 33615 Bielefeld, Germany

2   Working Group Fermentation and Formulation of Biologicals and Chemicals, Bielefeld Institute of Applied Materials Research, Bielefeld University of Applied Sciences, Interaktion 1, 33619 Bielefeld, Germany

an isoelectric point around 5.00 [21, 22]. The mechanism of release behavior of ions or drugs from gelatin-based polymers has been discussed in several articles [23, 24].

Meanwhile, cellulose is the most abundant naturally occurring polymer of glucose (Scheme 1a), which can be extracted from plants and natural fibers such as cotton and flax [25, 26]. The hydroxyl groups in the C-2 and C-5 positions of the cellulose chain can be chemically modified to form various functional groups such as primary amino groups ($-NH_2$), acetamide groups (CH_3CONH-), or carboxylate groups [27]. Among them, sodium carboxymethylcellulose (NaCMC, Scheme 1b), which contains negatively charged positions, is expected to favor slow release behavior due to electrostatic attraction with cations, which was used in our research in the formulation of SRF prototypes.

In addition to the electrostatic attraction between negatively charged positions and cations, water penetration and exchange due to the difference in nutrient concentration inside and outside fertilizers is the main mechanism for the release of nutrients from fertilizers into the soil. Thus, the open space for water determines the rate of water penetration or exchange, which affects the release rate of nutrients. Several studies applied this property to produce SRFs [17, 28–30].

However, gelatin and cellulose have been used either as coating materials for chemical fertilizers [28, 31, 32], or formulated separately with other polymers such as polyvinylpyrrolidone (PVP), poly(acrylamide), or dibutyl sebacate (DBS) as carriers for nutrients [15, 17, 33]. Neither was a study found reporting the formulation with these two degradable polymers as SRF, nor a paper discussing the release behavior of ions from the resulting polymer matrix, although these two polymers can be easily cross-linked by the Schiff base reaction (Scheme 2) to form hydrogels as suitable carriers that can absorb a lot of water and release it to the soil along with the nutrients among in the water, over a long time. This water retaining and slow release nature make hydrogels good candidates for SRFs [15, 34, 35].

In this study, we focused on the synthesis of hydrogels by the Schiff base reaction based on NaCMC with different degrees of substitution (DS) and gelatin (type B). The DS, the correlation length of hydrogel network as a measure of free volume, and the release kinetics of divalent iron cations (Fe^{2+}) from them under acidic conditions (pH = 3–4) typical for soils of our model plant blueberry were analyzed to understand whether the DS or the correlation length dominates the release rate of the cations.

Scheme 1 Chemical structure of **a** cellulose and **b** sodium carboxymethyl cellulose (NaCMC)
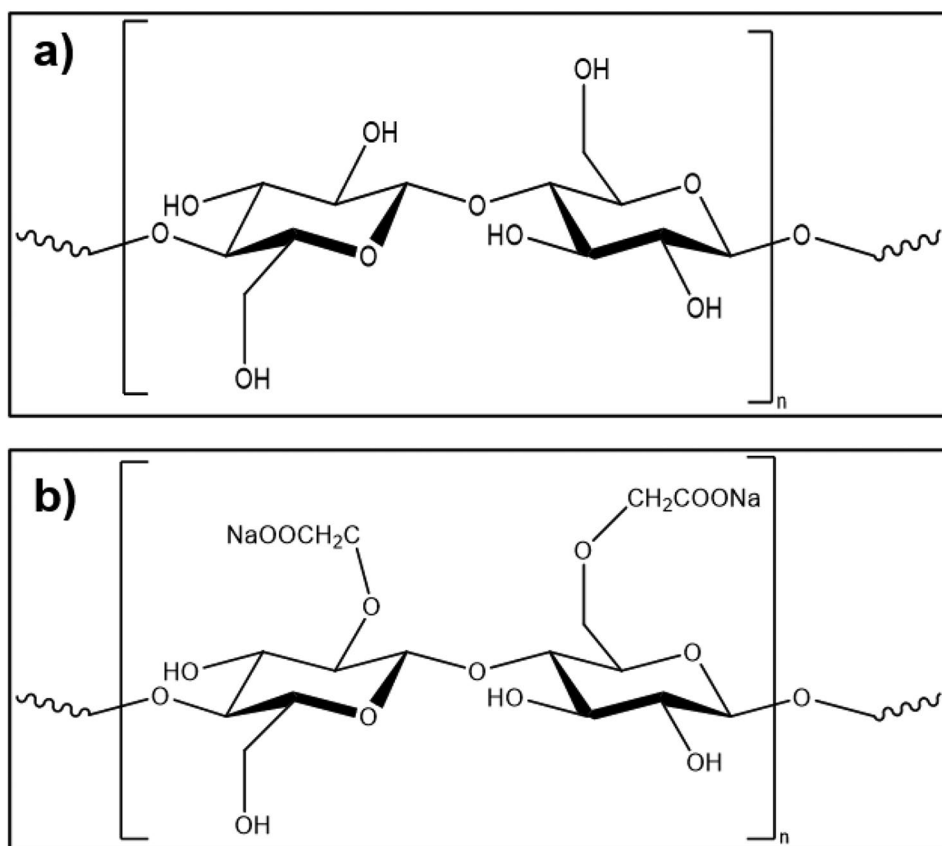
Scheme 2 General reaction mechanism of Schiff base reaction
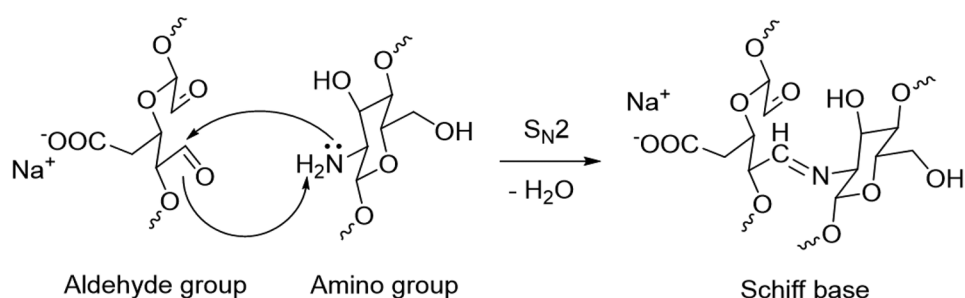
Materials and methods

Materials

Sodium carboxymethyl cellulose NaCMC-7 M, -9 M and -12 M (DS = 0.7, 0.9 and 1.2, M: medium viscosity, Ashland Company), gelatin (type B, IEP = 5, 100–180 kD, Gelita AG), sulfuric acid (96%, Carl Roth GmbH), sodium metaperiodate (99%, Carl Roth GmbH), ethylene glycol (99%, Carl Roth GmbH), hydroxylamine hydrochloride (99%, Thermo Scientific™), iron(II) sulphate heptahydrate (99.5%, Carl Roth GmbH). Dialysis membrane (Spectra/Pors, MWCO = 12–14 kDa). Deionized water was purified using an Arium pro VF system (Sartorius AG, Göttingen, Germany).

Preparation and characterization of dialdehyde carboxymethyl celluloses

Dialdehyde carboxymethyl cellulose (DACMC) was prepared according to the method of Jiang [36] and Zhang [37] with an optimized modification. The concentration of NaCMC solution was reduced to avoid incomplete mixing due to too high viscosity. The heating time was also extended to 24 h to ensure a complete reaction. For the three synthesis batches, 10 g of each of the three NaCMC (DS = 0.7, 0.9, or 1.2) were dissolved in 350 ml deionized water at 30 °C for 24 h. The pH of the NaCMC solutions was adjusted to 3.0 with 0.1 M H_2SO_4. Then, 10 g $NaIO_4$ in 100 ml deionized water (pH = 3.0) was slowly added to the NaCMC solutions under stirring. The mixtures were stirred at 30 °C for 72 h in the dark. After the remaining periodate was decomposed with 35 ml ethylene glycol for 30 min, the reaction solutions were dialyzed in deionized water for 3 days and freeze-dried using a freeze dryer (CHRIST Gefriertrocknungsanlage GmbH, Alpha 2–4 LSC basic) to gain the final product, namely DACMC-7 M, DACMC-9 M, and DACMC-12 M.

The IR spectrum of the DACMCs was recorded using a FT-IR spectrometer (JASCO 4100 with ATR, attenuated total internal reflection, crystal: zinc selenite) in the range of 4000–650 cm^{-1}.

Determination of the degree of oxidation of DACMCs

The degree of oxidation (DO) was estimated by hydroxylamine hydrochloride titration with an optimized modification [36–38]. 0.2 g of DACMC (7 M, 9 M, or 12 M) was dissolved in 15 ml deionized water. The pH of this solution was adjusted to 4.0 with 1.0 M NaOH. 8 ml 0.72 M hydroxylamine hydrochloride (pH = 4.0) was added to the DACMC solution and stirred at 40 °C for 4 h. The resulting hydrochloric acid was titrated with 1.0 M NaOH, and the consumption of the NaOH solution was recorded as V_c. NaCMC (DS = 0.7, 0.9, or 1.2) solution with the same concentration and pH was used as a blank, and the consumption of the 1.0 M NaOH solution was recorded as V_b. The DO of each DACMC was calculated using the following equation:

$$D.O.\% = \frac{M_{NaOH} \cdot (V_c - V_b)/2}{m/211} \tag{1}$$

where M_{NaOH} is 1.0 mol/l, m is the dry weight of DACMC, and *211* is the average molecular weight of the repeating units in DACMC. The estimation of DO was repeated three times for each DACMC.

Preparation and characterization of DACMC-gelatin hydrogels

In this study, different polymer ratios and total polymer contents were tried, but only the synthesis with a 5:1 polymer ratio (gelatin: DACMC) and a total polymer content of 10% proved successful in several replicates and was used for our study (see Supplementary information for details). The synthesis steps are as follows: 2.4 g of DACMC (7 M, 9 M, or 12 M) was dissolved in 96 ml of deionized water, and 12 g of gelatin (type B, IEP = 5, 100–180 kD, Gelita AG) was dissolved in 48 ml of deionized water. Both solutions were stirred at 60 °C for 1 h to obtain clear solutions. 1 ml of the gelatin solution was dropped separately into a 24-well plate, and then 2 ml of the DACMC solution was mixed well with the gelatin in the 24-well plate. The 24-well plate was then heated in an oven at 60 °C for 1 h. The synthesized

DACMC-Gelatin hydrogels (DG hydrogels) were removed from the 24-well plate, freeze-dried, and stored in a desiccator. The gelatin used to make all three hydrogels was the same with the same polymer concentration and ratio. The disk-shaped final products were named as DG-7, DG-9, and DG-12, depending on the type of three DACMCs used during synthesis. These hydrogels are intended for industrial scale agricultural use. Therefore, in this study the hydrogels are not washed after preparation, but used directly for the next experiments to better simulate of the manufacturing process in industry and the application conditions in agriculture.

The IR spectrum of DG hydrogels was recorded using a FT-IR spectrometer in the range of 4000–650 cm^{-1}.

Determination of gel fraction, swelling ratio, stability, and degradability of hydrogels

The measurement of gel fractions was performed and optimized following the article by Lam et al. [39]. The synthesized hydrogels were stored separately in 50 ml centrifuge tubes and completely freeze-dried in a freeze dryer. The percentage of gel fractions (GF%) was measured at 25 °C and calculated according to the following equation, where w_0 and w_1 are the weights of the original wet and dried hydrogels, respectively.

$$GF\% = \frac{w_1}{w_0} \cdot 100\% \tag{2}$$

The swelling ratio (SR) and the stability of hydrogels were determined in deionized water as follows. The as synthesized DG-7, DG-9, and DG-12 hydrogels were individually immersed in 25 ml of 0.1 M FeSO$_4$ solution separately at 25 °C for 48 h ($t_0 = -48$ h) to form the Fe-7, Fe-9, and Fe-12 hydrogels. The Fe-7, Fe-9, and Fe-12 hydrogels were then immersed in 25 ml of HCl-adjusted deionized water (pH = 3.5).

To determine the swelling ratio, the diameter d and thickness b of each disk-shaped hydrogel were measured with a caliper after a certain period of time, 5 different points were measured and averaged at a time, and the experiment was repeated three times for each hydrogel. The SR of Fe hydrogels were compared based on the growth volume calculated using the following equation:

$$V = b \cdot \pi \left(\frac{d}{2}\right)^2 \tag{3}$$

where V is the volume of the disc-shaped hydrogel, b reveals the thickness of each hydrogel, and d indicates the diameter of each hydrogel.

$$V\% = \frac{V_t}{V_0} \cdot 100\% \tag{4}$$

where V% is the volumetric swelling ratio, V_t is the volume of hydrogel at time t, and V_0 is the initial volume of each hydrogel before immersion in the FeSO$_4$ solution ($t_0 = -48$ h). The initial volume of the samples before swelling was recorded: V_0(DG-7) = 525.27 mm^3, V_0(DG-9) = 527.55 mm^3, V_0(DG-12) = 523.81 mm^3.

To determine the stability and degradability, the weight m of each hydrogel was recorded after a certain period of time. The ratio of weight change m% was calculated as follows:

$$m\% = \frac{m_t}{m_0} \cdot 100\% \tag{5}$$

where $m\%$ is the ratio of weight change, m_t is the weight of hydrogels after absorption in deionized water for time t, and m_0 is the initial weight of each hydrogel before immersion in FeSO$_4$ solution ($t_0 = -48$ h). The experiment was repeated three times for each hydrogel. The initial weight of the samples was recorded: m_0(DG-7) = 141 mg, m_0(DG-9) = 147 mg, m_0(DG-12) = 138 mg.

Each experiment was repeated three times.

Determination of correlation length of hydrogels with SAXS

Samples for small-angle X-ray scattering were prepared as follows: DG Hydrogels were immersed in 0.1 M FeSO$_4$ solution (pH = 3.47, named as Fe-7, Fe-9, and Fe-12) and HCl-adjusted deionized water (pH = 3) for 48 h. SAXS measurements were performed using an in-house SAXS/WAXS system (XEUSS, Xenocs, Sassenage, France) at room temperature. The hydrogel samples were cut into small pieces with a thickness of about 2 mm and measured in a solid sample holder. The corresponding excess sample solution was added to the cells, which were subsequently sealed with Kapton tape to prevent solvent evaporation during the measurement. Spectra were collected for 18 h per sample. Radial integration of the 2D detector image recorded by a Pilatus 300 K hybrid pixel detector (Dectris, Baden Deattwil, Switzerland) was performed using the Foxtrott software [40]. To obtain the scattered beam intensity on an absolute scale, background correction, and normalization with glassy carbon type 2 [41] were performed. Silver behenate reference sample, was used for the calibration to obtain exact q-values, with q being the magnitude of the scattering vector [42]:

$$q = \frac{4\pi}{\lambda} \sin\frac{\theta}{2} \tag{6}$$

with λ being the wavelength of the scattered light and θ the scattering angle. The scattering intensity was modeled using the approach of Saffer et al. utilizing the correlation length model to model the hydrogel SAXS Data as follows [43]:

$$I(q) = \frac{I_P(0)}{q^n} + \frac{I_B(0)}{1 + (q\xi)^m} \tag{7}$$

where I_P and I_B are scaling factors, q is the scattering vector. Parameters n, m, and ξ are the scattering exponent, the Lorentzian exponent, and the correlation length of the network fluctuations, respectively. For hydrogels, the correlation length of the polymer chains can also be referred to as the dynamics of the hydrogel. The scattering exponent gives information about the fractal structure of the gel network while the Lorentzian exponent depends on polymer solvent interactions [43–49].

Uptake and release kinetic of Fe²⁺ ions

To investigate the total amount of Fe loaded in hydrogels and the release kinetic of Fe²⁺ ions from hydrogels, 16 pieces of each DG hydrogel were weighed and placed in 50 ml centrifuge tubes separately. 25 ml 0.1 M FeSO₄ solution was poured into each centrifuge tube. After 48 h, the hydrogels (named as Fe-7, Fe-9, and Fe-12) were removed and carefully washed three times with exactly 2 ml deionized water. The solution used for immersion and washing was collected. The volume of the solution was measured and the concentration of Fe²⁺ ions in it was analyzed using an UV–Vis spectrometer (GENESYS 10S UV–Vis, Themo Fisher Scientific Inc.) and the total amount of Fe²⁺ absorbed in the hydrogel was calculated as follows:

$$n(Fe^{2+}) = 0.1M \cdot 0.025l \cdot M(Fe^{2+}) - c(Fe^{2+}) \cdot V \tag{8}$$

where $n(Fe^{2+})$ is the total amount of Fe²⁺ ions loaded into the hydrogel, $M(Fe^{2+})$ is the standard atomic weight of the iron atom, $c(Fe^{2+})$ indicates the concentration of Fe²⁺ ions in the solution and V is the volume of the solution.

The Fe hydrogels were then immersed separately in 25 ml HCl adjusted deionized water (pH = 3.5) in the 50 ml centrifuge tubes. After a period of time, the DG hydrogels were removed and the Fe²⁺ concentration in the remaining solution was determined by UV–Vis spectroscopy. The results were fitted using the modified Peleg's model considering the total amount of loaded Fe²⁺ in hydrogels as follows [50]:

$$E(t) = E_0 + \frac{t}{k_1 + k_2 t} \tag{9}$$

where $E(t)$ is the Fe²⁺ concentration at time t, E_0 reveals the initial concentration of Fe²⁺ ions at $t = 0$, k_1 is the temperature dependent Peleg's rate constant given as the percentage released as a function of time [51–53], and k_2 is Peleg's capacity constant at the equilibrium stage. According to Peleg et al., Noorolahi et al., and Abu-Ghannam et al., the reciprocal of k_1, i.e. value $1/k_1$ represents the release rate [50, 53–55].

Each experiment was repeated three times.

Results

### Preparation and characterization of DACMCs

Dialdehyde carboxymethyl cellulose (DACMC) was prepared by periodate oxidation with NaIO₄, to convert the unreactive hydroxyl groups in the polysaccharide to aldehyde groups, which can react with the amine groups for the consecutive gelation process (Scheme 3).

The structures of NaCMC and DACMCs were investigated by FT-IR and their spectra were shown in Fig. 1. It can be observed that all the DACMC samples exhibit two significant peaks at 1735 cm⁻¹ and 885 cm⁻¹ compared to the unoxidized NaCMC, confirming the introduction of aldehyde groups into the structure after periodate oxidation. The peak at 1735 cm⁻¹ represents the stretching vibration of the free dialdehyde group, while the peak at 885 cm⁻¹ is associated with the vibration of the hemiacetal group [56, 57]. The FT-IR spectra confirmed the successful synthesis of the DACMC products.

Determination of degree of oxidation (DO) of DACMCs

Since the aldehyde groups in DACMC are one of the important participants in the Schiff base reaction to form the hydrogels, their content may affect the correlation length of the formulated hydrogels. Scheme 4 shows the mechanism

Scheme 3 Oxidation reaction of sodium carboxymethyl cellulose (NaCMC) to dialdehyde carboxymethyl cellulose (DACMC). Reaction conditions: NaCMC:NaIO₄ = 1:1, 72 h, 30 °C, pH = 3
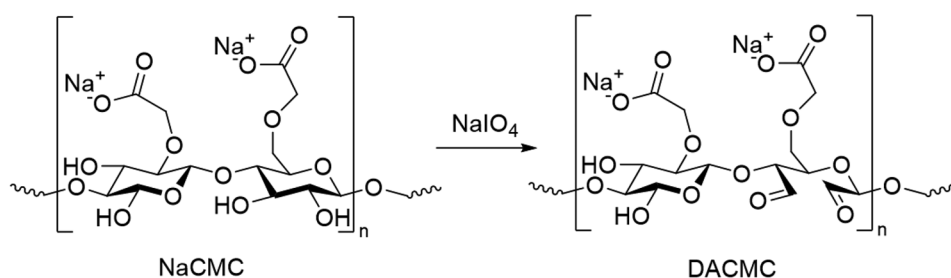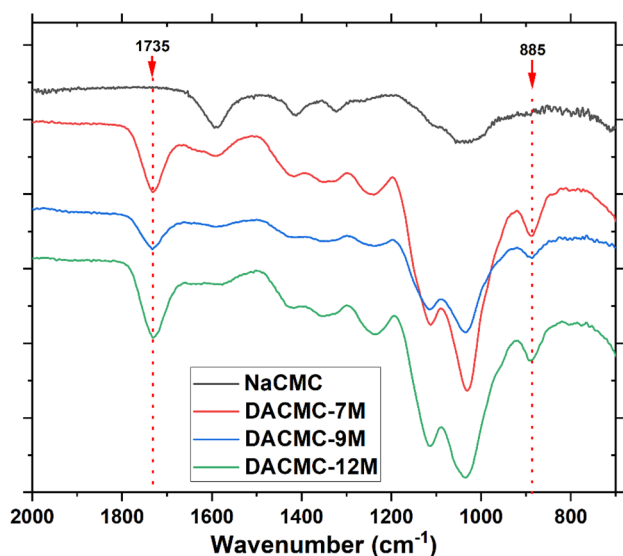
Fig. 1 *FT-IR* spectra (2000–700 cm^{-1}) of NaCMC (black), DACMC-7 M (red), 9 M (blue), and 12 M (green). 885 cm^{-1}: vibration of the hemiacetal group, 1735 cm^{-1}: vibration of the free dialdehyde group. The FT-IR spectra confirmed the successful synthesis of the DACMC products

for determination of the DO of DACMC with hydroxylamine hydrochloride. The DO of all DACMCs was calculated using Eq. 1, the results are shown in Fig. 2.

No significant difference was found among the three DACMCs, and the values were in a small interval between 13.10 and 13.35. In conclusion, the amount of carboxyl groups in the different celluloses did not affect the formation of aldehyde groups on the cellulose chain under the same reaction conditions, the DO of the DACMCs after oxidation were considered to be almost the same.

Preparation and characterization of DG hydrogels

DG hydrogels were synthesized by the Schiff base reaction between DACMC and gelatin. The aldehyde groups in DACMC and the primary amine groups in gelatin crosslinked with each other, leading to the formation of a three-dimensional network. The resulting C=N double bond is the sign of a Schiff base (Scheme 5).

The synthesized DG hydrogels are shown in Fig. 3a. The FT-IR spectra of the reactants and the corresponding DG

hydrogels are shown in Fig. 3b. The C=N bonds theoretically give rise to a peak in the range 1590–1690 cm^{-1}. However, the C=O stretching vibration of the carboxyl groups in DACMC generates a strong peak which may superimpose the C=N peak. Thus, the disappearance of the peaks at 1735 cm^{-1} and 885 cm^{-1}, revealing the disappearance of the aldehyde groups and the corresponding hemiacetal groups, is sufficient to demonstrate the successful formation of the C=N crosslinking point and the relevant Schiff base [58, 59].

## Determination of gel fraction, swelling ratio, stability, and degradability of hydrogels

The gel fractions of all DG hydrogels were calculated according to Eq. 2. The results are shown in Fig. 4.

From the graph, we can see that the gel fractions of all three hydrogels are almost the same, ranging from 15% to 16%. Based on this data, we infer that the total content and ratio of DACMC and gelatin in the three synthesized hydrogels are also similar.

The swelling ratio of hydrogels reflects the ability to absorb water, which also affects the release kinetics of ions [60]. In this research, the swelling ratio of three Fe hydrogels was determined by the volume growth of the disk-shaped hydrogels according to Eqs. 3 and 4, which was calculated based on their thickness b and diameter d (Fig. 5a). The results are shown in Fig. 5b.

The swelling ratios of all three hydrogels reached equilibrium after about 14 days (336 h) and showed no significant decrease until day 35 (840 h), reflecting the stability of the Fe hydrogels in acidic solutions (pH = 3.5). The swelling ratio of the Fe-12 hydrogel was the largest among the three, with a volume expansion of about 2.4 times the initial volume, while the swelling ratio of the Fe-7 hydrogel was the smallest, at about 2 times the initial volume. The Fe-12 sample has better water absorption capacity compared to the other two hydrogels, but this may also lead to faster diffusion of ions from it. From day 42 (1008 h), a slow decrease in the swelling ratio of the Fe-12 sample was observed, while the swelling ratio of Fe-7 and Fe-9 did not decrease, also indicating that the structures of Fe-7 and Fe-9 hydrogels are more stable compared to Fe-12.

Scheme 4 Mechanism for determination of DO of DACMC with NH$_2$OH·HCl
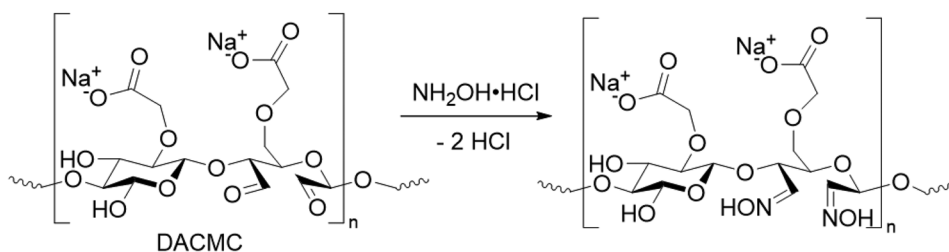
Fig. 2 Degree of oxidation of three DACMCs formulated by oxidation with $NaIO_4$ ($n = 3$). The DO of the DACMCs after oxidation were considered to be almost the same
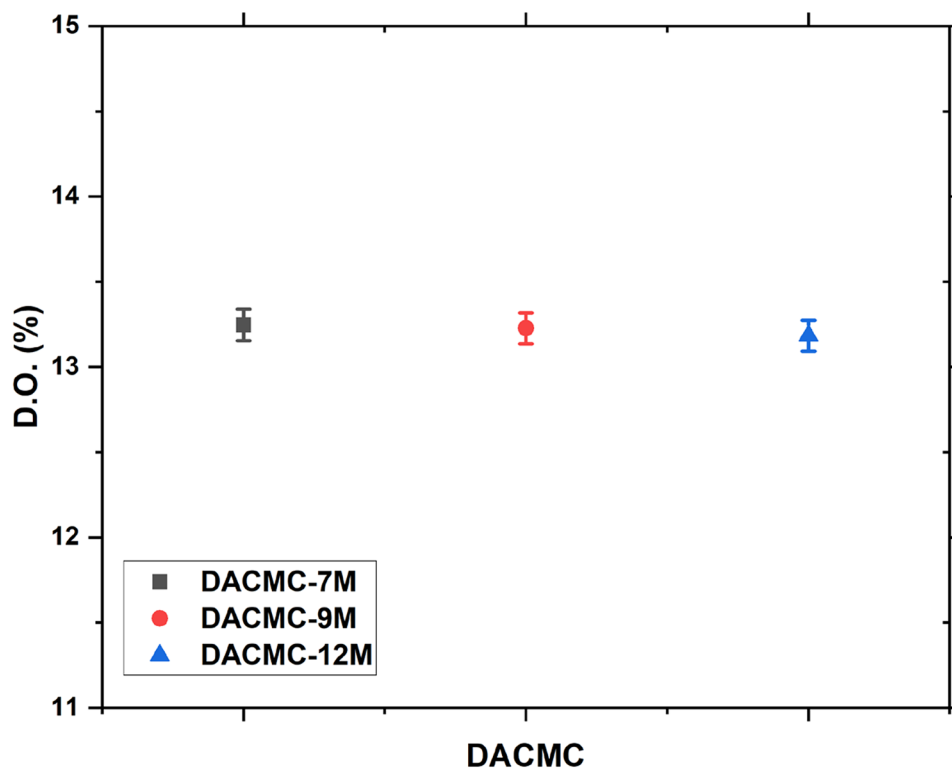

The stability of the hydrogels helps to avoid the bursting effect caused by damage of the hydrogel structure, which improves the slow-release ability of the SRFs [19, 61], while the degradable hydrogels avoid the accumulation of the polymer matrix in the soil, which causes deterioration of the soil environment [17, 18]. The weight changes of the hydrogels were determined using Eq. 5 and the results were summarized in Fig. 6.

As shown in Fig. 6, the trends of weight changes of the three Fe hydrogels coincided with the trends of volume changes in Fig. 5. On the 31st (744 h), the weight change ratio of the three hydrogels attained the maximum, with the weight change ratio of the Fe-12 hydrogel reaching 9.4 times the initial weight, which was higher than that of Fe-9 (7.6 times) and Fe-7 (7.3 times). Like the swelling ratio results, this also suggests that the Fe-12 hydrogel can absorb more water. This could be due to its looser internal structure,

which likely results in a higher diffusion rate of iron ions from the gel. From day 42 (1008 h), the weight change ratios of Fe-9 and Fe-12 began to decrease, with the weight change ratio of Fe-12 decreasing more significantly, indicating that a significant degradation process of Fe-12 began at this time. In contrast, the weight change ratio of Fe-7 showed no significant downward trend, indicating that its structure in acidic solution was more stable than the other two.

In summary, all three hydrogels exhibited long-term stability (35 days) in an aqueous solution with pH = 3.5. Among them, the Fe-12 hydrogel showed a better ability to absorb water, but this could be due to its looser internal structure, which also leads to a higher diffusion rate of ions from it, which is unfavorable for a slow-release fertilizer. The Fe-7 hydrogel has some disadvantage in water uptake compared to the other two hydrogels, but its stability is better, which is more favorable for slow-release

Scheme 5 Schiff base reaction mechanism of DACMC and gelatin
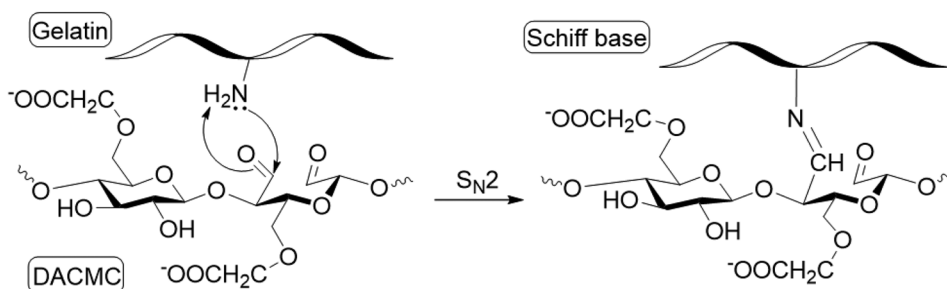
Fig. 3 **a** Freeze-dried DG hydrogels DG-7, DG-9, and DG-12, and **b** *FT-IR* spectra (2000–800 cm^{-1}) of DACMC (green), gelatin (purple), DG-7 (black), DG-9 (red), and DG-12 (blue). 885 cm^{-1}: vibration of the hemiacetal group, 1735 cm^{-1}: vibration of the free dialdehyde group. The disappearance of the aldehyde groups and the corresponding hemiacetal groups demonstrate the successful formation of the C=N crosslinking point and the relevant Schiff base
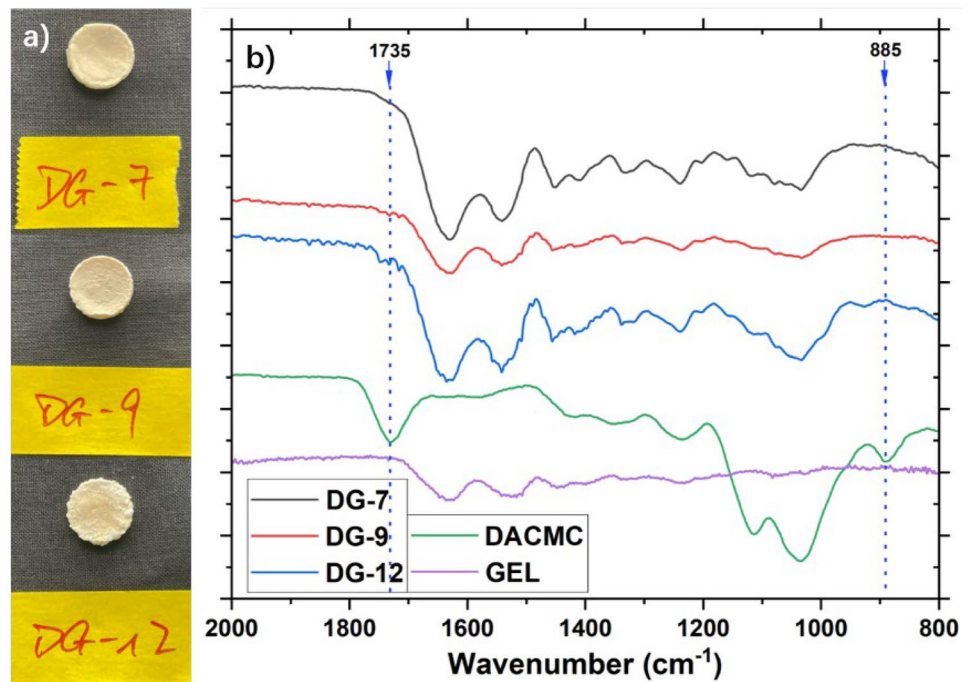

fertilizer. All three hydrogels showed a tendency to degrade after 42 days, with Fe-12 showing the most significant degradation. In contrast, the degradation of Fe-7 was slower, so the burst effect caused by too rapid degradation was better avoided.

## Determination of correlation length of hydrogels with SAXS

In this study, the correlation length ξ *o*f the synthesized hydrogels was investigated to describe the mesh size of the polymer.

Fig. 4 Gel fractions (GF%) for DG-7, DG-9, and DG-12 hydrogels after freeze-drying (*n* = 3)
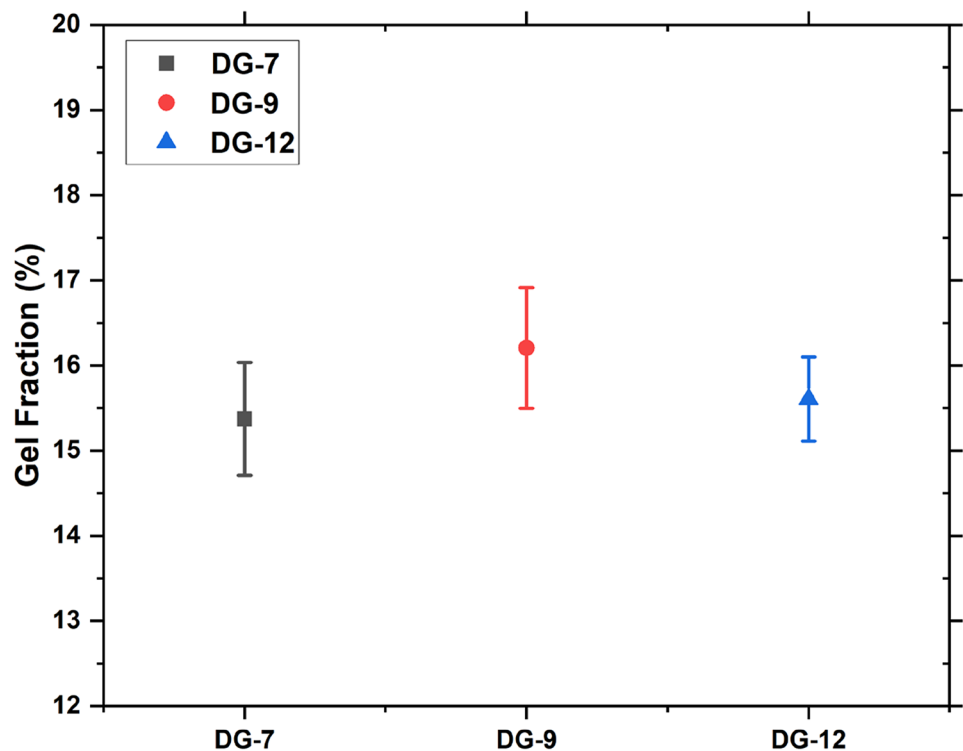
Fig. 5 **a** Diameter d and thickness b of an Fe hydrogel and **b** swelling ratio of Fe-7 (black), Fe-9 (red), and Fe-12 (blue) up to 42 days calculated by corresponding diameter d and thickness b at pH = 3.5 ($n = 3$)
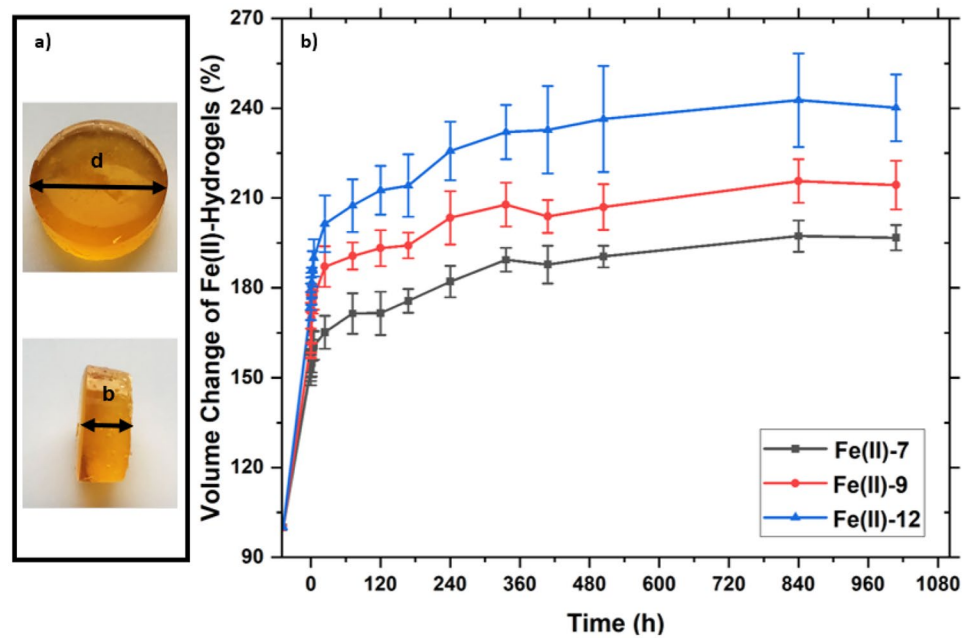
For some cross-linked hydrogels a second correlation length ξ_c can be found. It reveals the average distance between two adjacent crosslinking points (Scheme 6) [43, 46, 47]. In our case, a large ξ_c may be due to the low content of primary amine groups in gelatin, which offers only a low number of reaction points for Schiff base formation with aldehyde groups in DACMCs and causes dispersed crosslinking points.

The fitting parameters of the SAXS measurements are summarized in Table 1.

Figure 7 shows SAXS data which were fitted by Eq. 7. The distance between the crosslinking points (ξ_c) cannot be resolved in our experiments which is most-likely due to the rather low number of them. To take the increasing signal at low q into account, the increased scattering intensity at low

Fig. 6 Weight change ratio of Fe-7 (black), Fe-9 (red), and Fe-12 (blue) by 42 days at pH = 3.5 ($n = 3$)
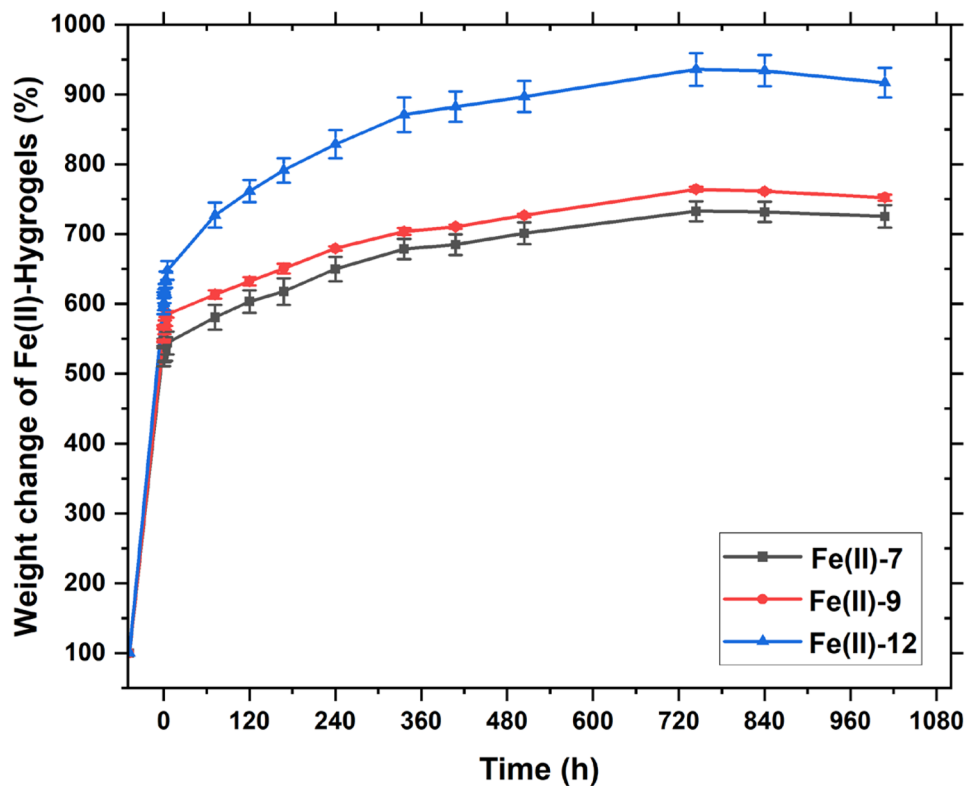
Scheme 6 Representation of water-absorbed DG hydrogel networks. ξ_c and ξ_d indicate the correlation length illustrated through average distance between crosslinking points or mesh size caused by additional aggregative interactions in hydrogel, respectively
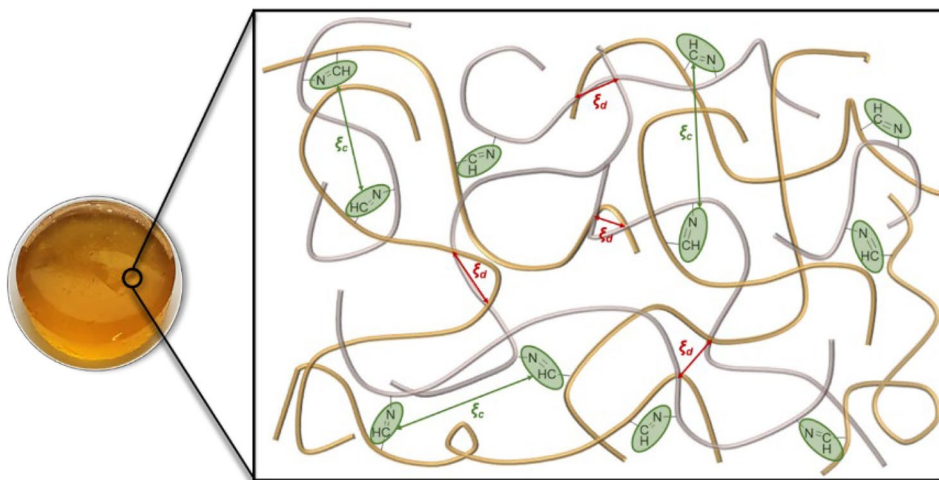
q is modeled by a power law in Eq. 7. This procedure does not give us any information about ξ_c, which could only be measured in q regions unavailable for us, and was done only to fit the data in the low q region. However, the scattering exponent n gives information about the structure of the gel.

An exponent of $n = 4$ would satisfy the Debye-Bueche relation and is caused by the crosslinking of the hydrogels, while exponents in the region of $n = 3$ to 4 denote a mass fractal structure of the gel, caused by additional aggregative interactions [62].

In this work we observe $n = 4$ for DG-12 and Fe-9, indicating no mass fractal, while the gels with fewer carboxyl groups seem to have a mass fractal structure. One reason for that could be the electrostatic repulsion between the carboxyl groups preventing aggregation.

The most important information obtained from the SAXS graphs is the dynamic mesh size ξ. In general, the dynamic mesh size of DG-12 was larger than the dynamic mesh sizes of DG-9 and far larger than DG-7, especially after the introduction of Fe^{2+} cations (Fig. 8a). This shows that the hydrogel chains in DG-12 have a more extended polymer network structure. This trend is due to the higher portion of carboxyl groups in DACMC-12 M. The electrostatic repulsion with the hydrogel networks is enhanced and the corresponding ξ of DG-12 was larger than DG-9 and DG-7 at the same

polymer concentration. One reason for the difference in the dynamic mesh size ξ of the individual hydrogels in $FeSO_4$ solution compared to their dynamic mesh size in deionized water may be the introduction of more negative sulfate anions, which resulted in higher electrostatic repulsion. This appears to have little effect on the dynamic mesh size of Fe-9 and Fe-7. For Fe-12, there is a significant increase in ξ, which can be attributed to the higher content of carboxyl groups. In addition, the fact that Fe-12 has the largest swelling ratio among all hydrogels is consistent with the fact that it has the largest correlation length.

Overall, DG-12 and Fe-12 showed the largest dynamic mesh size among the three hydrogels, which is attributed to higher electrostatic repulsion, especially after absorption in $FeSO_4$ solution. This is not only the reason for the largest swelling ratio of DG-12, but may also lead to a higher ion release rate from Fe-12.

Uptake and release kinetic of Fe^{2+} ions

The total amount of Fe^{2+} cations in the Fe hydrogels is shown in Fig. 9. Of the three hydrogels, Fe-12 absorbed more Fe^{2+} cations, about 20% more in total than Fe-9 and Fe-7. Fe-12 has a better ion absorption capacity, which is most likely due to its looser structure and correspondingly better ability to absorb more water. However, this difference in Fe^{2+}-loadings does not have a very significant effect on ion release, and the concentrations of loaded Fe^{2+} ions in the hydrogels were already taken into account when fitting the release rate using Eq. 9.

The release kinetic of Fe^{2+} cations from the hydrogels into the water (Fig. 8b) was investigated by UV–Vis measurement of the released Fe^{2+} concentration per unit volume of the hydrogel in a given time period with the concentration-absorption correlation of the Fe^{2+} standard solution and fitted according to Peleg's model (Eq. 9). Peleg's rate constant k_1 is

Table 1 Fit parameters of the SAXS measurements based on Eq. 2

Sample	$I_P / cm^{-1} \cdot 10^{-7}$	I_B / cm^{-1}	n	m	$\xi / \mathring{A}$
DG-7	2.00	2.19	3.75	2.15	27.26
DG-9	1.09	2.26	3.51	2.23	29.49
DG-12	0.32	3.22	4.00	1.95	31.69
Fe-7	2.00	6.49	3.37	3.13	25.33
Fe-9	0.01	6.33	4.00	3.31	27.75
Fe-12	0.14	15.85	3.30	3.21	37.30

Fig. 7 Fit of the SAXS results of **a** DG-7, DG-9, and DG-12 in deionized water (pH=3) and **b** Fe-7, Fe-9, and Fe-12 in FeSO$_4$ solution (pH=3.47)
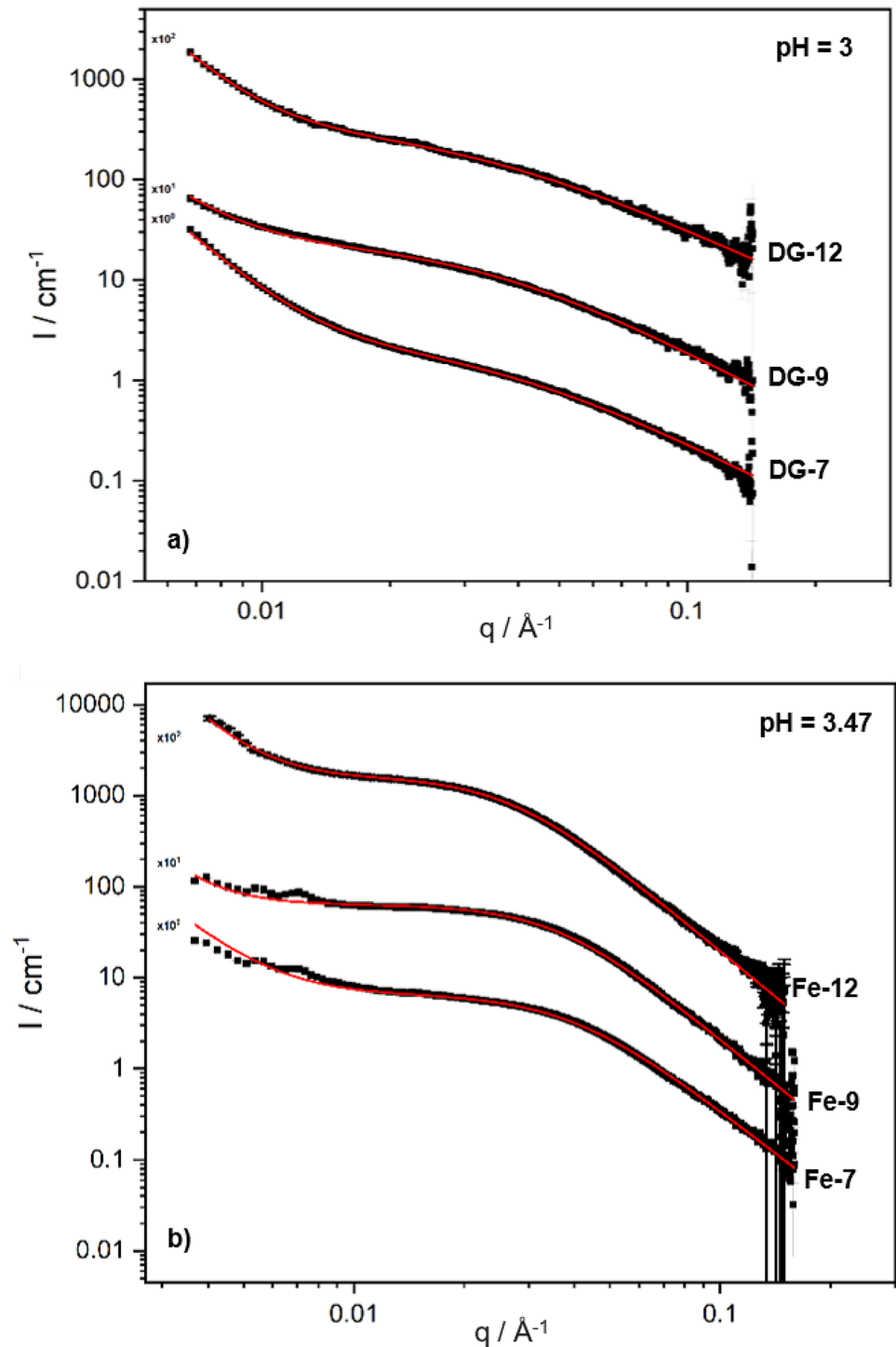

confirmed to be related only to the temperature according to Peleg et al., Hung et al., and Sopade et al. [51, 52]. Since the gelatin used for the formulation has the same polymer concentration and ratio for all three hydrogels, its effect on the release behavior of Fe ions is also considered to be the same in this study. The release results are analyzed together with the correlation length and DS of DACMCs to understand which of these two parameters dominates the release kinetic of Fe^{2+} cations.

The Fe-12 hydrogel released the highest amount of Fe^{2+} cations among the three hydrogels in a given time period. After fitting with Peleg's model, the $1/k_1$ value of each hydrogel, which reveals the release rate of Fe^{2+} cations, is shown in Fig. 10 in dependence on the correlation length of each hydrogel.

Fig. 8 **a** Dynamic mesh size of DG hydrogels after swelling in water (DG-7, DG-9, and DG-12) and in FeSO$_4$ solution (Fe-7, Fe-9, and Fe-12). **b** Release kinetics of Fe-7, Fe-9, and Fe-12 fitted with Peleg's model (Eq. 9) in the 1st hour by pH = 3.5 (*n* = 3)
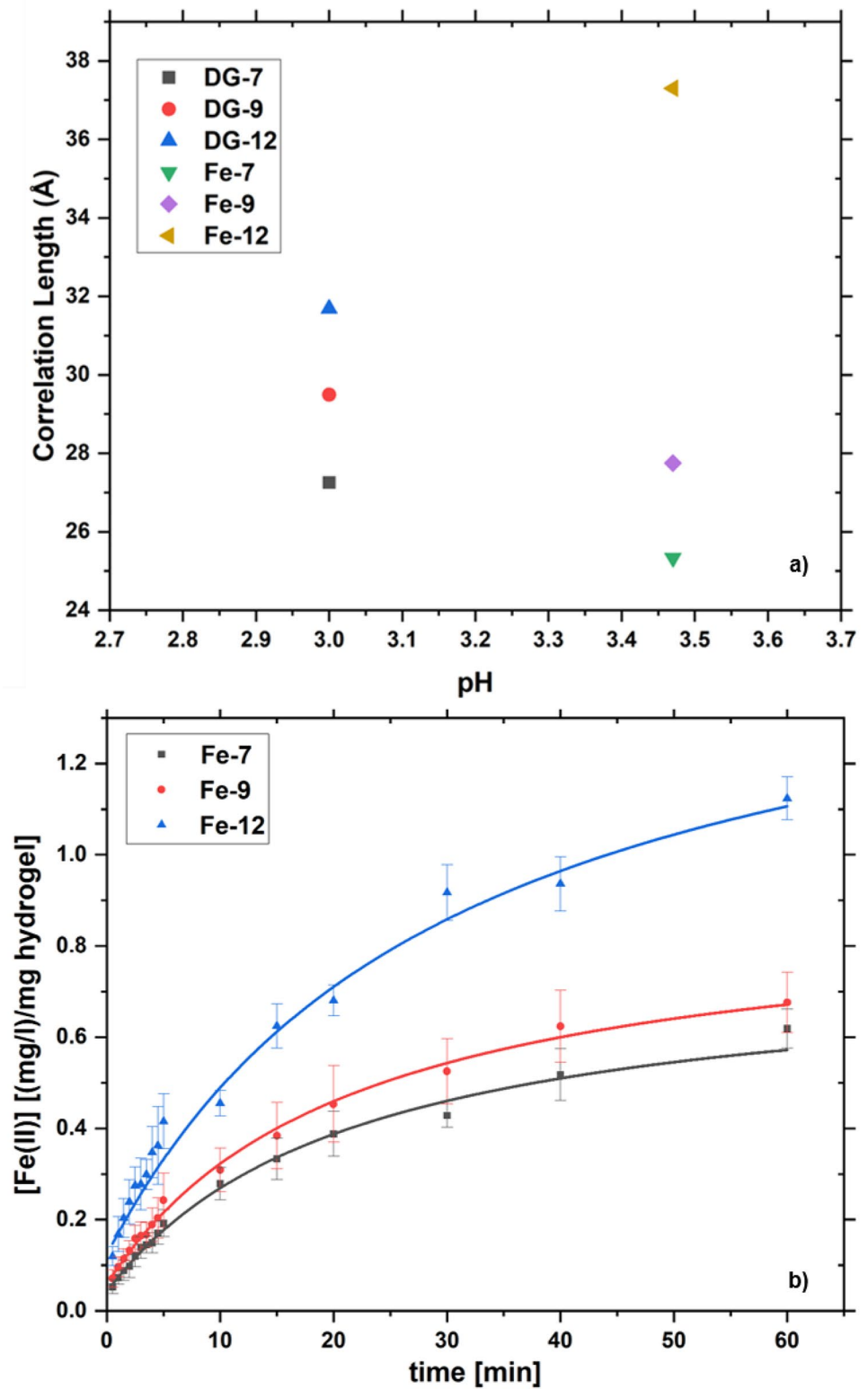
Fig. 9 Total amount of Fe^{2+} cations in different Fe hydrogels ($n = 3$)
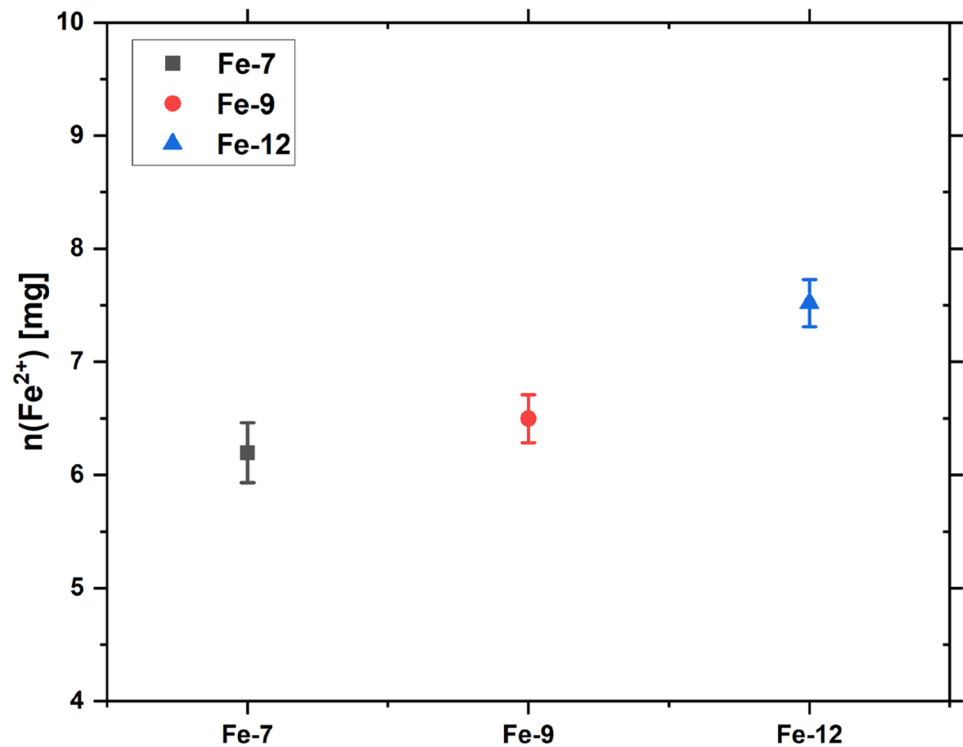
According to Fig. 9, the release rate of Fe^{2+} from Fe-12 was almost 1.5 times as fast as from Fe-7 and 1.3 times as fast as from Fe-9. The dynamic mesh size ξ of Fe-12 was confirmed to be much larger than Fe-7 and Fe-9 (Fig. 8a) and the release rate of Fe^{2+} from DG hydrogels increases with increasing dynamic mesh size. Thus, it is demonstrated that the dynamic mesh size is the decisive parameter for the release rate of Fe^{2+} from DG hydrogels, while the electrostatic attraction between carboxyl groups and cations shows less or no influence at pH 3.5.

Fig. 10 Release kinetics in dependence on the correlation length (dynamic mesh size) of the hydrogels Fe-7, Fe-9, and Fe-12 by pH 3.5 ($n = 3$)
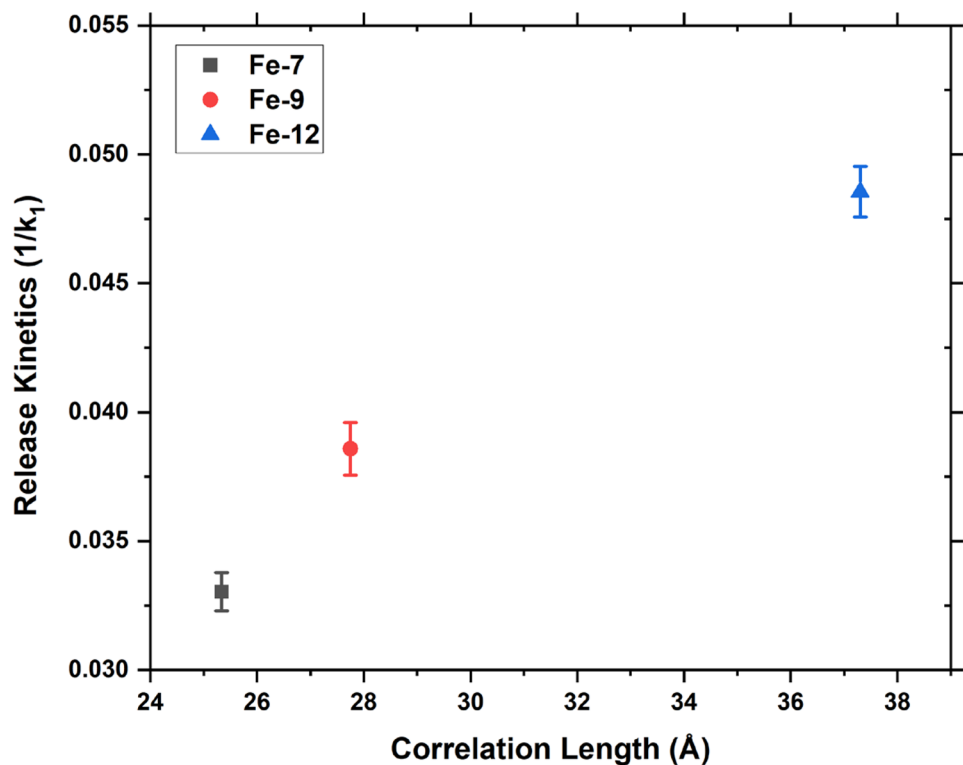
Conclusion

In this study, DG hydrogels based on oxidized carboxymethyl cellulose and gelatin were successfully synthesized and characterized. The stability and degradability after absorption of Fe ions were analyzed. Hydrogels with various contents of carboxyl groups show different release speeds of Fe^{2+} cations. The correlation length of hydrogels and degree of substitution of carboxyl groups in cellulose were analyzed and the dynamic mesh size (correlation length) is revealed to be a decisive parameter for the release rate of Fe^{2+} cations.

The hydrogels were found to have long-term stability, and were slowly but continuously degradable over time at lower pH value. It was found that Fe-12 degraded faster than Fe-9 and Fe-7. We assume a less stable structure caused by the hindrance of the formation of crosslinking points between DACMC-12 M and gelatin due to the higher content of negative carboxyl groups during the synthesis. Since the gelatin used to formulate all three hydrogels has the same polymer concentration and ratio, its effect on the hydrogel structure is also considered to be the same. Thus, in this study, the difference in the DS of the DACMCs is considered to be the only reason for the differences in the swelling ratios and weight changes of the three hydrogels. DG-12 which contains the most negatively charged positions, exhibits the highest electrostatic repulsion between the polymer chains, resulting in a looser and therefore more degradable structure. In contrast, DG-7 exhibits the lowest electrostatic repulsion between the polymer chains and therefore the tightest structure. The addition of divalent Fe ions increases the ionic strength [63, 64] of the external solution resulting in a lower mesh size for Fe-7 and Fe-9 compared to DG-7 and DG-9. As an exception to the expected trend, Fe-12 shows a small increase in mesh size compared to DG-12, indicating another unknown interaction that may play a role here.

Fe-12 with the highest DS and the largest correlation length showed the highest release rate of Fe^{2+} cations. A higher content of carboxyl groups, i.e., a higher DS, can provide electrostatic attraction with cations and thereby reduce the release rate of Fe^{2+} cations. However, such an effect on the release rate should not be observed because the pH was adjusted to 3.5, which resulted in suppression of any electrostatic effects produced by deprotonated carboxyl groups. In contrast, this resulted in a higher repulsion between the polymer chains and a larger distance between the polymer chains within the hydrogel structure, which also led to a higher degree of swelling and a larger correlation length. Therefore, the penetration and exchange of water together with the cations were faster in Fe-12 than Fe-9 and Fe-7 and resulted in the highest release speed of cations. The water-retaining and slow-release behavior as well as the degradability of the three formulated hydrogels at lower pH indicated their potential as slow-release fertilizers. The smallest correlation length and the most compact structure, as well as the slowest degradation, were found for the Fe-7 hydrogel, which favors the slow release of iron ions and avoids the burst effect caused by too fast degradation, making it the most suitable candidate for slow-release fertilizers.

Our next step is to analyze the release kinetics of other cations with different charges such as K^+, Ca^{2+}, Fe^{3+}, or anions such as PO_4^{3-}. In future works, the correlation length and release behavior of DG hydrogels at higher pH will be studied. Since carboxyl groups in cellulose will be deprotonated at higher pH, we expect electrostatic interactions between the cations and the deprotonated carboxyl groups to gain importance, which may lead to slower release kinetics for DG-12.

Declarations

Competing interests The authors declare no competing interests.

References

1. Araújo BR, Romão LPC, Doumer ME, Mangrich AS (2017) Evaluation of the interactions between chitosan and humics in media for the controlled release of nitrogen fertilizer. J Environ Manage 190:122–131. https://doi.org/10.1016/j.jenvman.2016.12.059. (PMID: 28040588)

2. Avelino F, Miranda IP, Moreira TD et al (2019) The influence of the structural features of lignin-based polyurethane coatings on ammonium sulfate release: kinetics and thermodynamics of the process. J Coat Technol Res 16(2):449–463. https://doi.org/10.1007/s11998-018-0123-y

3. Global Network Against Food Crises (2022) Global Report on Food Crises 2022. World Food Programme (WFP). https://www.wfp.org/publications/global-report-food-crises-2022. Accessed 21 Apr 2023

4. Azeem B, KuShaari K, Man ZB, Basit A, Thanh TH (2014) Review on materials & methods to produce controlled release coated urea fertilizer. J Control Release 181:11–21. https://doi.org/10.1016/j.jconrel.2014.02.020. (PMID: 24593892)

5. Timilsena YP, Adhikari R, Casey P, Muster T, Gill H, Adhikari B (2015) Enhanced efficiency fertilisers: a review of formulation and nutrient release patterns. J Sci Food Agric 95(6):1131–1142. https://doi.org/10.1002/jsfa.6812. (PMID: 25043832)

6. Majeed Z, Ramli NK, Mansor N, Man Z (2015) A comprehensive review on biodegradable polymers and their blends used in controlled-release fertilizer processes. Rev Chem Eng 31(1). https://doi.org/10.1515/revce-2014-0021

7. Guo M, Liu M, Hu Z, Zhan F, Wu L (2005) Preparation and properties of a slow release NP compound fertilizer with superabsorbent and moisture preservation. J Appl Polym Sci 96(6):2132–2138. https://doi.org/10.1002/app.21140

8. Boyandin AN, Kazantseva EA, Varygina DE, Volova TG (2017) Constructing slow-release formulations of ammonium nitrate fertilizer based on degradable poly(3-hydroxybutyrate). J Agric Food Chem 65(32):6745–6752. https://doi.org/10.1021/acs.jafc.7b01217. (PMID: 28723220)

9. Altomare C, Tringovska I (2011) Beneficial soil microorganisms, an ecological alternative for soil fertility management. Sustain Agric Res 7:161–214

10. Dhaliwal SS, Naresh RK, Mandal A et al (2019) Effect of manures and fertilizers on soil physical properties, build-up of macro and micronutrients and uptake in soil under different cropping systems: a review. J Plant Nutr 42(20):2873–2900. https://doi.org/10.1080/01904167.2019.1659337

11. Lehmann A, Veresoglou SD, Leifheit EF, Rillig MC (2014) Arbuscular mycorrhizal influence on zinc nutrition in crop plants – a meta-analysis. Soil Biol Biochem 69:123–131. https://doi.org/10.1016/j.soilbio.2013.11.001

12. Levett I, Pratt S, Donose BC et al (2019) Understanding the mobilization of a nitrification inhibitor from novel slow release pellets, fabricated through extrusion processing with PHBV biopolymer. J Agric Food Chem 67(9):2449–2458. https://doi.org/10.1021/acs.jafc.8b05709. (PMID: 30724561)

13. Wu L, Liu M (2008) Preparation and properties of chitosan-coated NPK compound fertilizer with controlled-release and water-retention. Carbohydr Polym 72(2):240–247. https://doi.org/10.1016/j.carbpol.2007.08.020

14. Liu Q-R, Qi J-R, Yin S-W et al (2016) The influence of heat treatment on acid-tolerant emulsions prepared from acid soluble soy protein and soy soluble polysaccharide complexes. Food Res Int 89(Pt 1):211–218. https://doi.org/10.1016/j.foodres.2016.07.001. (PMID: 28460907)

15. Bortolin A, Aouada FA, de Moura MR, Ribeiro C, Longo E, Mattoso LHC (2012) Application of polysaccharide hydrogels in adsorption and controlled-extended release of fertilizers processes. J Appl Polym Sci 123(4):2291–2298. https://doi.org/10.1002/app.34742

16. Guilherme MR, Aouada FA, Fajardo AR et al (2015) Superabsorbent hydrogels based on polysaccharides for application in agriculture as soil conditioner and nutrient carrier: a review. Eur Polymer J 72:365–385. https://doi.org/10.1016/j.eurpolymj.2015.04.017

17. Olad A, Zebhi H, Salari D, Mirmohseni A, Reyhani TA (2018) Slow-release NPK fertilizer encapsulated by carboxymethyl cellulose-based nanocomposite with the function of water retention in soil. Mater Sci Eng C Mater Biol Appl 90:333–340. https://doi.org/10.1016/j.msec.2018.04.083. (PMID: 29853099)

18. Kottegoda N, Sandaruwan C, Perera P, Madusanka N, Karunaratne V (2015) Modified layered nanohybrid structures for the slow release of urea. NANOASIA 4(2):94–102. https://doi.org/10.2174/2210681204021505211124729

19. Madusanka N, Sandaruwan C, Kottegoda N et al (2017) Urea–hydroxyapatite-montmorillonite nanohybrid composites as slow release nitrogen compositions. Appl Clay Sci 150:303–308. https://doi.org/10.1016/j.clay.2017.09.039

20. Santoro M, Tatara AM, Mikos AG (2014) Gelatin carriers for drug and cell delivery in tissue engineering. J Control Release 190:210–218. https://doi.org/10.1016/j.jconrel.2014.04.014. (PMID: 24746627)

21. Echave MC, Sánchez P, Pedraz JL, Orive G (2017) Progress of gelatin-based 3D approaches for bone regeneration. J Drug Deliv Sci Technol 42:63–74. https://doi.org/10.1016/j.jddst.2017.04.012

22. Yamamoto M, Ikada Y, Tabata Y (2001) Controlled release of growth factors based on biodegradation of gelatin hydrogel. J Biomater Sci Polym Ed 12(1):77–88. https://doi.org/10.1163/156856201744461. (PMID: 11334191)

23. Boppana R, Kulkarni RV, Mutalik SS, Setty CM, Sa B (2010) Interpenetrating network hydrogel beads of carboxymethylcellulose and egg albumin for controlled release of lipid lowering drug. J Microencapsul 27(4):337–344. https://doi.org/10.3109/02652040903191842. (PMID: 20163285)

24. Li J, Wang Y, Zhang L, Xu Z, Dai H, Wu W (2019) Nanocellulose/gelatin composite cryogels for controlled drug release. ACS Sustainable Chem Eng 7(6):6381–6389. https://doi.org/10.1021/acssuschemeng.9b00161

25. Islam S, Bhuiyan MAR, Islam MN (2017) Chitin and chitosan: structure, properties and applications in biomedical engineering. J Polym Environ 25(3):854–866. https://doi.org/10.1007/s10924-016-0865-5

26. Rahman Bhuiyan MA, Hossain MA, Zakaria M, Islam MN, Zulhash UM (2017) Chitosan coated cotton fiber: physical and antimicrobial properties for apparel use. J Polym Environ 25(2):334–342. https://doi.org/10.1007/s10924-016-0815-2

27. Kabir SMF, Sikdar PP, Haque B, Bhuiyan MAR, Ali A, Islam MN (2018) Cellulose-based hydrogel materials: chemistry, properties and their prospective applications. Prog Biomater 7(3):153–174. https://doi.org/10.1007/s40204-018-0095-0. (PMID: 30182344)

28. Li Y, Da Zhen, Liao S, Zhu D, Yang X (2018) Controlled-release urea encapsulated by ethyl cellulose/butyl acrylate/vinyl acetate hybrid latex. Pol J Chem Technol 20(4):108–12. https://doi.org/10.2478/pjct-2018-0062

29. Xiang Y, Ru X, Shi J et al (2017) Preparation and properties of a novel semi-IPN slow-release fertilizer with the function of water retention. J Agric Food Chem 65(50):10851–10858. https://doi.org/10.1021/acs.jafc.7b03827. (PMID: 29172492)

30. Xie L, Liu M, Ni B, Zhang X, Wang Y (2011) Slow-release nitrogen and boron fertilizer from a functional superabsorbent formulation based on wheat straw and attapulgite. Chem Eng J 167(1):342–348. https://doi.org/10.1016/j.cej.2010.12.082

31. Ni B, Liu M, Lü S, Xie L, Wang Y (2011) Environmentally friendly slow-release nitrogen fertilizer. J Agric Food Chem 59(18):10169–10175. https://doi.org/10.1021/jf202131z. (PMID: 21848295)

32. Qiao D, Liu H, Yu L et al (2016) Preparation and characterization of slow-release fertilizer encapsulated by starch-based superabsorbent polymer. Carbohydr Polym 147:146–154. https://doi.org/10.1016/j.carbpol.2016.04.010. (PMID:27178919)

33. Pérez-García S, Fernández-Pérez M, Villafranca-Sánchez M, González-Pradas E, Flores-Céspedes F (2007) Controlled release of ammonium nitrate from ethylcellulose coated formulations. Ind Eng Chem Res 46(10):3304–3311. https://doi.org/10.1021/ie061530s

34. Bortolin A, Aouada FA, Mattoso LHC, Ribeiro C (2013) Nanocomposite PAAm/methyl cellulose/montmorillonite hydrogel: evidence of synergistic effects for the slow release of fertilizers. J Agric Food Chem 61(31):7431–7439. https://doi.org/10.1021/jf401273n. (PMID: 23822729)

35. Leone G, Delfini M, Di Cocco ME, Borioni A, Barbucci R (2008) The applicability of an amidated polysaccharide hydrogel as a cartilage substitute: structural and rheological characterization. Carbohydr Res 343(2):317–327. https://doi.org/10.1016/j.carres.2007.10.017. (PMID: 18039540)

36. Jiang X, Yang Z, Peng Y et al (2016) Preparation, characterization and feasibility study of dialdehyde carboxymethyl cellulose as a novel crosslinking reagent. Carbohydr Polym 137:632–641. https://doi.org/10.1016/j.carbpol.2015.10.078. (PMID: 26686173)

37. Zhang Y, Zhang L, Shao S, Chang X, Li M (2020) Periodate oxidation of carboxymethyl cellulose under controlled conditions. ChemistrySelect 5(22):6765–6773. https://doi.org/10.1002/slct.202000470

38. Hofreiter BT, Alexander BH, Wolff IA (1955) Rapid estimation of dialdehyde content of periodate oxystarch through quantitative alkali consumption. Anal Chem 27(12):1930–1931. https://doi.org/10.1021/ac60108a023

39. Lam YL, Muniyandy S, Kamaruddin H, Mansor A, Janarthanan P (2015) Radiation cross-linked carboxymethyl sago pulp hydrogels loaded with ciprofloxacin: influence of irradiation on gel fraction, entrapped drug and in vitro release. Radiat Phys Chem 106:213–222. https://doi.org/10.1016/j.radphyschem.2014.07.018

40. Viguier G, Girardot R, Perez J (2016) Foxtrot 3.3.4

41. Zhang F, Ilavsky J, Long GG, Quintana J, Allen AJ, Jemian PR (2010) Glassy carbon as an absolute intensity calibration standard for small-angle scattering. Metall Mater Trans A 41A:1151–1158

42. Huang TC, Toraya H, Blanton TN, Wu Y (1993) X-ray powder diffraction analysis of silver behenate, a possible low-angle diffraction standard. J Appl Crystallogr 26(2):180–184. https://doi.org/10.1107/S0021889892009762

43. Saffer EM, Lackey MA, Griffin DM, Kishore S, Tew GN, Bhatia SR (2014) SANS study of highly resilient poly(ethylene glycol) hydrogels. Soft Matter 10(12):1905–1916. https://doi.org/10.1039/c3sm52395k. (PMID: 24652367)

44. Hammouda B, Horkay F, Becker ML (2005) Clustering and solvation in poly(acrylic acid) polyelectrolyte solutions. Macromolecules 38(5):2019–2021. https://doi.org/10.1021/ma047960g

45. Hule RA, Nagarkar RP, Hammouda B, Schneider JP, Pochan DJ (2009) Dependence of self-assembled peptide hydrogel network structure on local fibril nanostructure. Macromolecules 42:7137–7145

46. Hule RA, Nagarkar RP, Altunbas A et al (2008) Correlations between structure, material properties and bioproperties in self-assembled beta-hairpin peptide hydrogels. Faraday Discuss 139:251–64; discussion 309–25, 419–20. https://doi.org/10.1039/b717616c. (PMID: 19048999)

47. Matsunaga T, Sakai T, Akagi Y, Chung U, Shibayama M (2009) SANS and SLS studies on tetra-arm PEG gels in as-prepared and swollen states. Macromolecules 42(16):6245–6252. https://doi.org/10.1021/ma901013q

48. Hammouda B, Ho DL, Kline S (2004) Insight into clustering in poly(ethylene oxide) solutions. Macromolecules 37:6932–6937

49. Karg M, Hellweg T (2012) Smart microgel/nanoparticle hybrids with tunable optical properties. In: Luis Andrew Lyon, Michael Serpe, editor. Hydrogel Micro and Nanoparticles. 1st ed. Weinheim: Wiley-VCH pp 257–79

50. Vargas-Ruiz S, Schulreich C, Kostevic A et al (2016) Extraction of model contaminants from solid surfaces by environmentally compatible microemulsions. J Colloid Interface Sci 471:118–126. https://doi.org/10.1016/j.jcis.2016.03.006. (PMID: 26994352)

51. Hung TV, Liu LH, Black RG, Trewhella MA (1993) Water absorption in chickpea (C. arietinum) and field pea (P. sativum) cultivars using the Peleg model. J Food Sci 58(4):848–52

52. Sopade PA, Obekpa JA (1990) Modelling water absorption in soybean, cowpea and peanuts at three temperatures using Peleg's equation. J Food Sci 55(4):1084–1087

53. Peleg M (1988) An Empirical Model for the Description of Moisture Sorption Curves. J Food Sci 53(4):1216–1219

54. Abu-Ghannam N, McKenna B (1997) The application of Peleg's equation to model water absorption during the soaking of red kidney beans. J Food Eng 32(4):391–401

55. Noorolahi S, Khazaei J, Jafari S (2008) Modeling cyclic water absorption and desorption characteristics of three varieties of wood. IAALD AFITA WCCA

56. Lei J, Li X, Wang S et al (2019) Facile fabrication of biocompatible gelatin-based self-healing hydrogels. ACS Appl Polym Mater 1(6):1350–1358. https://doi.org/10.1021/acsapm.9b00143

57. Li H, Wu B, Mu C, Lin W (2011) Concomitant degradation in periodate oxidation of carboxymethyl cellulose. Carbohydr Polym 84(3):881–886. https://doi.org/10.1016/j.carbpol.2010.12.026

58. Du S, Chen X, Chen X et al (2019) Covalent chitosan-cellulose hydrogels via Schiff-base reaction containing macromolecular microgels for pH-sensitive drug delivery and wound dressing. Macromol Chem Phys 220(23):1900399. https://doi.org/10.1002/macp.201900399

59. Sethi S, Kaith BS, Kaur M, Sharma N, Khullar S (2020) A hydrogel based on dialdehyde carboxymethyl cellulose–gelatin and its utilization as a bio adsorbent. J Chem Sci 132(1). https://doi.org/10.1007/s12039-019-1700-z

60. Liang R, Liu M (2006) Preparation and properties of a double-coated slow-release and water-retention urea fertilizer. J Agric Food Chem 54(4):1392–1398. https://doi.org/10.1021/jf052582f. (PMID: 16478265)

61. González ME, Cea M, Medina J et al (2015) Evaluation of biodegradable polymers as encapsulating agents for the development of a urea controlled-release fertilizer using biochar as support material. Sci Total Environ 505:446–453. https://doi.org/10.1016/j.scitotenv.2014.10.014. (PMID: 25461046)

62. Horkay F, Basser PJ, Hecht A-M, Geissler E (2005) Structural investigations of a neutralized polyelectrolyte gel and an associating neutral hydrogel. Polymer 46(12):4242–4247. https://doi.org/10.1016/j.polymer.2005.02.054

63. Yang X, Dargaville BL, Hutmacher DW (2021) Elucidating the molecular mechanisms for the interaction of water with polyethylene glycol-based hydrogels: influence of ionic strength and gel network structure. Polymers (Basel) 13(6). https://doi.org/10.3390/polym13060845. (PMID: 33801863)

64. Vigata M, Meinert C, Bock N, Dargaville BL, Hutmacher DW (2021) Deciphering the molecular mechanism of water interaction with gelatin methacryloyl hydrogels: role of ionic strength, pH, drug loading and hydrogel network characteristics. Biomedicines 9(5). https://doi.org/10.3390/biomedicines9050574. (PMID: 34069533)